

EVIDENCE FOR COLD ACCRETION: PRIMITIVE GAS FLOWING ONTO A GALAXY AT $Z \sim 0.274$ ¹

JOSEPH RIBAUDDO^{2,3}, NICOLAS LEHNER², J. CHRISTOPHER HOWK², JESSICA K. WERK⁴, TODD M. TRIPP⁵, J. XAVIER PROCHASKA⁴, JOSEPH D. MEIRING⁵, & JASON TUMLINSON⁶

Accepted for publication in ApJ

ABSTRACT

We present UV and optical observations from the Cosmic Origins Spectrograph on the *Hubble Space Telescope* and Keck of a $z = 0.27395$ Lyman limit system (LLS) seen in absorption against the QSO PG1630+377. We detect H I absorption with $\log N(\text{H I}) = 17.06 \pm 0.05$ as well as Mg II, C III, Si III, and O VI in this system. The column densities are readily explained if this is a multi-phase system, with the intermediate and low ions arising in a very low metallicity ($[\text{Mg}/\text{H}] = -1.71 \pm 0.06$) photoionized gas. We identify via Keck spectroscopy and Large Binocular Telescope imaging a $0.3 L_*$ star-forming galaxy projected 37 kpc from the QSO at nearly identical redshift ($z = 0.27406$, $\Delta v = -26$ km s⁻¹) with near solar metallicity ($[\text{O}/\text{H}] = -0.20 \pm 0.15$). The presence of very low metallicity gas in the proximity of a near-solar metallicity, sub- L_* galaxy strongly suggests that the LLS probes gas infalling onto the galaxy. A search of the literature reveals that such low metallicity LLSs are not uncommon. We found that 50% (4/8) of the well-studied $z \lesssim 1$ LLSs have metallicities similar to the present system and show sub- L_* galaxies with $\rho < 100$ kpc in those fields where redshifts have been surveyed. We argue that the properties of these primitive LLSs and their host galaxies are consistent with those of cold mode accretion streams seen in galaxy simulations.

Subject headings: Galaxies: Evolution—Intergalactic Medium—Quasars: Absorption lines

1. INTRODUCTION

Galaxies are predicted to acquire the majority of their baryons through cold,⁷ filamentary streams that penetrate deep inside the dark matter halos without shock-heating to the virial temperature (Birnboim & Dekel 2003; Kereš et al. 2005). This so-called cold mode accretion (CMA) may be the primary mechanism by which galaxies acquire material needed for star formation from the intergalactic medium (IGM) (Bauermeister et al. 2010). Such streams are predicted to have low temperatures ($T \sim 10^4$ K), low metallicities (averaging $\langle Z \rangle \sim 0.001 - 0.01 Z_\odot$ depending on the simulation), and to be predominantly ionized (Fumagalli et al. 2011; Faucher-Giguère & Kereš 2011). CMA models predict such streams will remain cold only for galaxies below a threshold mass $M_{\text{Halo}} \lesssim 10^{12} M_\odot$ (or $M_* \sim 5 \times 10^{10} M_\odot$; Kereš et al. 2005; Stewart et al. 2010). Estimates of the covering factor of cold streams within the virial radius for such galaxies range from 5% up to 40%, depending on redshift and model parameters. Despite the fundamental role CMA may play in galaxy formation and evolution, observations have provided little direct evidence for its

existence.

QSO absorption lines can probe the circumgalactic medium of foreground galaxies, with intermediate H I column density systems ($15.5 \leq \log N(\text{H I}) \leq 19.0$) being particularly promising tracers of cold accretion streams (e.g., Fumagalli et al. 2011; Faucher-Giguère & Kereš 2011). Among these, LLSs with $\log N(\text{H I}) \geq 16.5$ are both readily identifiable and often allow for straightforward H I column density measurements due to the flux discontinuity they cause at the Lyman limit (912 Å in the rest frame). The use of LLSs to probe infalling and outflowing matter near galaxies has the advantage that they are selected in a metallicity-independent manner. Thus, unlike searches for Mg II and other metal line-selected absorbers, LLS searches are not biased in favor of either metal-enriched winds or infalling matter in galaxy halos. Furthermore, when the strength of the Lyman break is not too strong (i.e., $\tau \lesssim 3$), the H I column density of the system can be measured, from which the metallicity and, ultimately, the origins of the absorbing gas can be determined. These features circumvent some of the problems that currently cause disagreements in the interpretation of the strong Mg II-selected absorbers, for which some studies suggest the absorbers trace outflowing material while others suggest they may represent infalling material (Bouché et al. 2007; Ménard & Chelouche 2009; Chen et al. 2010; Bowen & Chelouche 2011; Kacprzak et al. 2011).

Recent surveys of LLSs have examined the statistical nature of the absorber population, delineating the redshift evolution of these absorbers (Prochaska et al. 2010; Songaila & Cowie 2010; Ribaud et al. 2011). The literature contains only a few LLSs for which the physical properties of the gas (metallicity, ionization structure, kinematics) and the host galaxy (luminosity, metallicity, mass) are well con-

¹ Based on observations with the NASA/ESA Hubble Space Telescope obtained at the Space Telescope Science Institute, which is operated by the Association of Universities for Research in Astronomy, Incorporated, under NASA contract NAS5-26555.

² Department of Physics, University of Notre Dame, Notre Dame, IN 46556

³ Current Address: Department of Physics, Utica College, Utica, NY, 13502

⁴ UCO/Lick Observatory, University of California, Santa Cruz, Santa Cruz, CA 95064

⁵ Department of Astronomy, University of Massachusetts, Amherst, MA 01003

⁶ Space Telescope Science Institute, Baltimore, MD 21218

⁷ Cold here implies the gas is not heated to the virial temperature; however, the temperature of the gas ($\sim 10^4$ K) is well above that of the cold material in the disk of the galaxy.

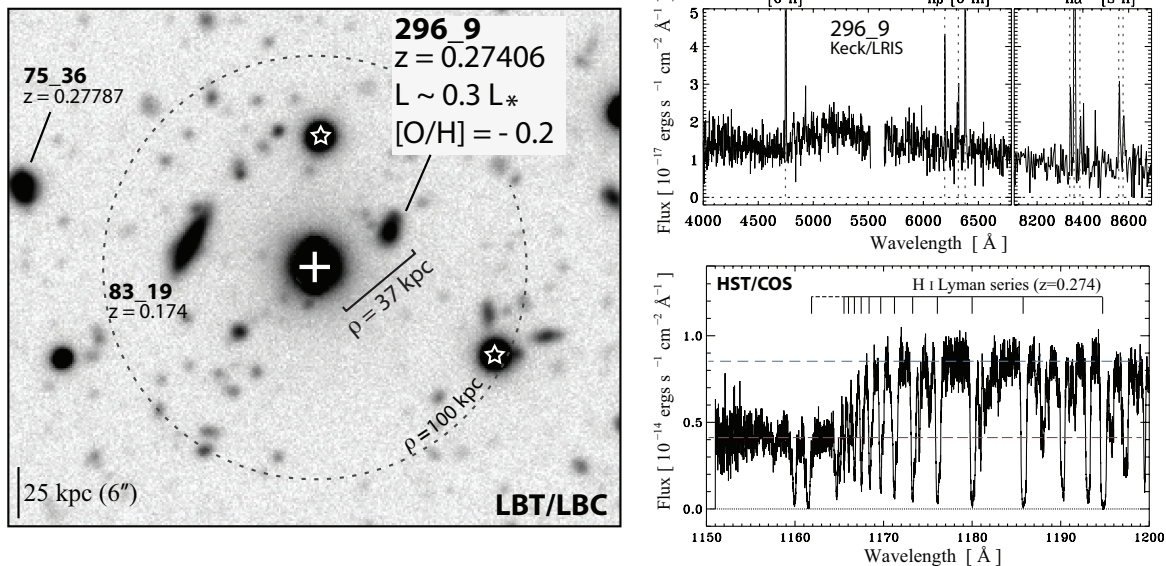


FIG. 1.— A small section of a 2.5 ks LBT *g*-band image of the PG1630+377 field (left). The dashed circle shows a 100 kpc radius ($\sim 25''$) about the QSO at $z = 0.274$. The host galaxy candidate is labeled 296_9 and is a projected 37 kpc from the QSO line of sight (marked with a +). Other galaxies in the field with spectroscopic redshifts are noted. Foreground stars are marked with a star symbol. The LRIS spectrum of galaxy 296_9 (upper right) shows the emission lines characteristic of a star forming galaxy. A portion of the COS spectrum of PG1630+377 (lower right) shows the LLS located at $z = 0.27395$ and the Lyman series lines leading up to the break. The H I column density of the LLS ($\log N(\text{H I}) = 17.06 \pm 0.05$) was calculated by comparing the estimated unabsorbed continuum flux (upper dashed line) and the estimated mean absorbed flux (lower dashed line).

strained (Chen & Prochaska 2000; Jenkins et al. 2005; Tripp et al. 2005; Prochaska et al. 2006; Cooksey et al. 2008; Lehner et al. 2009; Tumlinson et al. 2011). To understand the implications for the statistical evolution of LLSs in the context of galaxy evolution it is necessary to better understand the gas-galaxy relationship, including the frequency with which LLSs trace infall onto versus outflows from galaxies.

Here we use observations from the Cosmic Origins Spectrograph (COS), with additional ground-based spectroscopic and imaging observations, to analyze a LLS at $z \sim 0.274$ along the sight line to the UV-bright QSO PG1630+377 ($z_{\text{em}} = 1.476$). We demonstrate the LLS has low metallicity (§ 2) and use Large Binocular Telescope (LBT) imaging and Keck spectroscopy of galaxies in the QSO field to identify a near-solar metallicity, $0.3 L_*$ galaxy at virtually the same redshift (§ 3). We discuss this gas in the context of cold mode accretion models in § 4 and summarize our results in § 5.

2. ABSORPTION FROM THE LOW METALLICITY LYMAN LIMIT SYSTEM

The UV spectra of PG1630+377 were obtained with COS on-board the *Hubble Space Telescope* (PID 11741, PI Tripp) using the G130M (1150–1450 Å) and G160M (1405–1775 Å) gratings. The exposure times for these two configurations were 23.0 and 14.3 ks, respectively, giving S/N up to 30–40 per resolution element at unabsorbed wavelengths. The excellent quality of the UV spectra is displayed in Figures 1 and 2. The data were processed using CALCOS (v2.11b) and coadded following Meiring et al. (2011). The lower-right panel of Figure 1 shows a small portion of the spectrum obtained from COS, highlighting the presence of a LLS at $z \sim 0.274$. Optical spectra were obtained with HIRES at the Keck Observatory on 26 March 2010 and cover Mg II $\lambda\lambda 2796, 2803$ at $z \sim 0.274$. We acquired 3 HIRES

exposures totaling 2.2 ks under good conditions with the blue cross-disperser, the C1 decker (0.86'' width giving FWHM $\approx 6 \text{ km s}^{-1}$), and the CCD mosaic. The data were processed using HIReDux in IDL.⁸

Figure 2 shows the normalized absorption profiles of H I (*left panels*) and metal ions (*right panels*) as a function of velocity relative to $z_{\text{abs}} = 0.27395$, the centroid of Mg II absorption. At $v = 0 \text{ km s}^{-1}$ we detect H I, C III, Si III, weak Mg II absorption ($W_r(2796) = 59 \pm 4 \text{ mÅ}$), and possibly O VI. We refer to this as the strong component⁹ due to the strength of the H I absorption. Near $v = +50 \text{ km s}^{-1}$ ($z = 0.27416$) we detect H I, C III, Si III, and O VI, but no Mg II. We refer to this as the weak component. In Figure 3 we show the apparent column density profiles, $N_a(v)$ (Savage & Sembach 1991), of selected species. This figure demonstrates that the O VI follows the intermediate ion Si III and H I in the weak component well and that all of the observed O VI could be due to the weak component.

The column densities and limits for selected species can be found in Table 1. We determine the column densities of metal ions by integrating their $N_a(v)$ profiles. For non-detections, we quote 3σ limits following Lehner et al. (2008). From the flux decrement at the Lyman limit, we measure the total optical depth of the system to be $\tau_{\text{LLS}} = 0.73 \pm 0.08$ (see Figure 1), implying a total H I column density $\log N(\text{H I}) = 17.06 \pm 0.05$ (see Spitzer 1978). We determine the H I column density of the weak component by integrating the $N_a(v)$ profiles of the weak, unsaturated Lyman series lines. The top panel in Figure 3 shows the contrast in the saturation effect between the two components: for the weak component, the weak

⁸ <http://www.ucolick.org/~xavier/HIReDux/index.html>

⁹ Though we use the term components, the reader should be aware each is likely an unresolved blend of multiple sub-components or “clouds.”

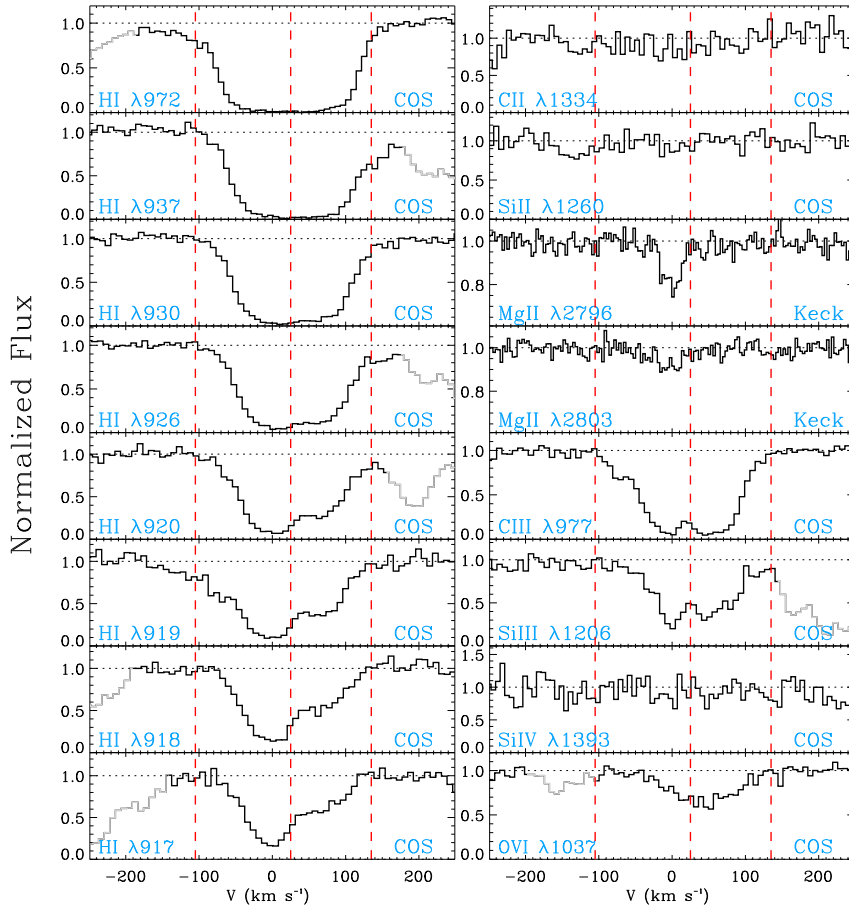


FIG. 2.— Plots of absorption lines as a function of velocity centered on the LLS at $z=0.27395$. The H I Lyman series is shown on the left-hand side, while the right-hand side shows the metal ions. The dashed lines show the low ion integration limits adopted for the strong ($[-105, +25]$ km s^{-1}) and weak components ($[+25, +135]$ km s^{-1}). We do not detect C II, Si II, or Si IV in either component. The O VI $\lambda 1031$ is largely contaminated by another unrelated absorber and is not reproduced here. Gray portions of the spectra are absorption from unrelated absorbers. Note the scale of the panels showing the Mg II lines are set to a different scale than the rest of the panels.

Lyman series lines provide a good estimate of the H I column density. We find $\log N(\text{H I}) = 16.30 \pm 0.02$ for the weak component. The column density of the strong component is the difference between the total and weak component column densities, $\log N(\text{H I}) = 16.98 \pm 0.06$. As a consistency check, we have also fitted the H I absorption profiles with a two component model, wherein a model absorption profile is convolved with the COS instrumental spread function to determine the best fit values of the central velocities, column densities, and Doppler parameters of the two assumed components. The columns derived from such profile fitting models are consistent with the integrated values, while the b -values for both components are about 30 km s^{-1} . We emphasize, however, that the results from profile fitting depend upon the assumed component structure of the gas. While we have assumed a two component model, each is quite likely made up of several blended absorbing components.

To determine the metallicity and physical conditions of the strong component, we model its ionization using Cloudy (v08.01, Ferland et al. 1998). We assume the gas is photoionized, modeling it as a uniform slab in thermal and ionization equilibrium. We illuminate the slab with the Haardt & Madau (2011) background radiation field from quasars and galaxies. We vary the ionization parameter, $U = n_\gamma/n_H$, and metallicity of the gas (assum-

ing solar relative abundances from Asplund et al. (2009)) to match the observed column density constraints (Table 1).

We summarize the results of the Cloudy simulations for the strong component in Figure 4. The ionization parameter is very well constrained by the adjacent ionization states of Si and C, while the metallicity of the gas is fixed mostly by Mg II. The observed column densities are reproduced for models with an ionization parameter $\log U = -2.80 \pm 0.30$, which is represented by the green shaded region in the upper panel. This $\log U$ gives a metallicity of $[\text{Mg}/\text{H}] = -1.71 \pm 0.06$. For this range of $\log U$ the gas is almost completely ionized, with a neutral hydrogen fraction, $X(\text{H I}) = N(\text{H I})/N(\text{H}) \sim 0.001 - 0.004$. The particle density in these models is $n_H \sim 0.001 - 0.003 \text{ cm}^{-3}$, the total H column is $\log N(\text{H}) \sim 19.6$, the physical size of the absorbing cloud is $L = N_H/n_H \sim 2-25 \text{ kpc}$, and the temperature of the gas is predicted to be $T \sim (2 - 4) \times 10^4 \text{ K}$. This temperature is consistent with the component fitting where $b(\text{H I}) \sim 30 \text{ km s}^{-1}$ which implies a temperature of $\sim 3 \times 10^4 \text{ K}$. We note that the ionization state of this gas is unusually well constrained by the lack of either Si II or Si IV absorption and the presence of strong Si III.

The intermediate and low ions in the weak component can be described by similar photoionization mod-

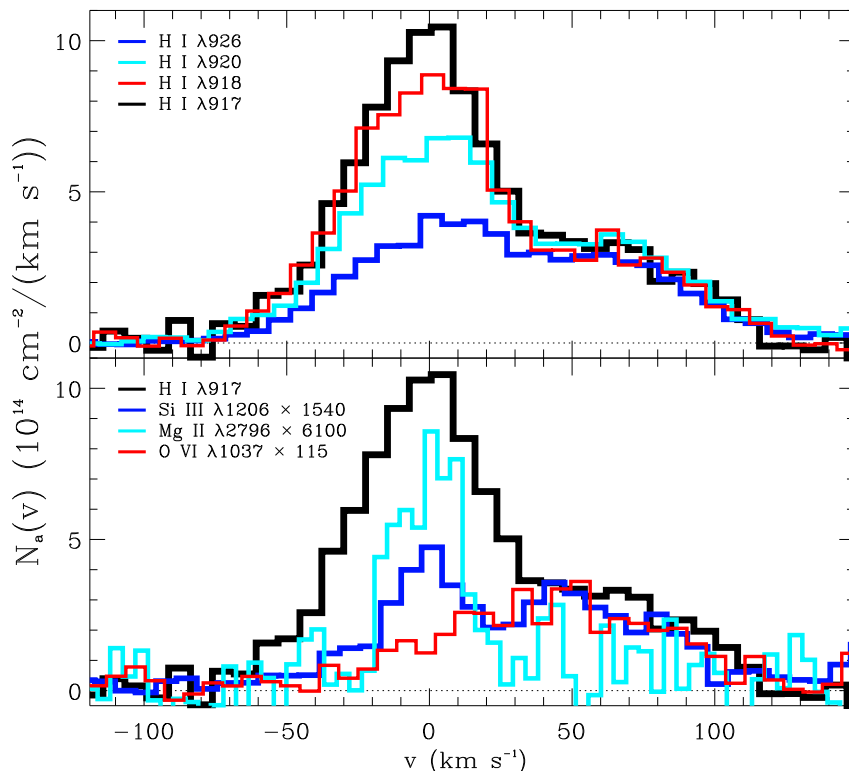


FIG. 3.— The apparent column densities of several H I transitions (*top panel*) and H I and metal ions (*bottom panel*). The top panel shows the different effects of saturation on the two main components of H I, specifically the weak H I component is unsaturated. In the bottom panel, the apparent column densities of the ions have been scaled, revealing that (i) the H I and weak/intermediate aligns well in the strong component, and (ii) the O VI follows the lower ions and H I of the weak component extremely well.

els with a metallicity consistent with the strong component. However, this does not explain the strong O VI absorption. We hypothesize the weak component is a multiphase structure in which low-metallicity gas is interacting directly with the gaseous corona of the host galaxy (§ 3). In this scenario the O VI is produced in the interface between the low-ionization gas and the corona, analogous to the O VI seen in the Galactic high velocity clouds (Sembach et al. 2003). The close kinematic relationship of the intermediate and high ion profiles (Figure 3) is consistent with this hypothesis (Howk et al. 2009). The close kinematic relationship of the intermediate and high ion profiles, however, could also suggest another possibility in which all the ions trace the same gas. The ionic ratios (C III/O VI, Si III/O VI, Si III/H I) can be matched by nonequilibrium models (Gnat & Sternberg 2007) if the metallicity of the gas is near solar. In this case, the weak component would represent radiatively-cooling material associated with the host galaxy. The close correspondence between the O VI and the H I in the weak component is not unusual; at low redshifts, O VI and H I absorption profiles are often observed to be well-aligned and to have similar profile shapes (Tripp et al. 2008).

3. THE GALACTIC ENVIRONMENT OF THE LYMAN LIMIT SYSTEM

The left panel of Figure 1 shows a *g*-band image of the field toward PG1630+377 obtained with the Large Binocular Camera (LBC) on the LBT. The 2.5 ks LBC image was taken with $\sim 1''$ seeing and reaches 5σ limiting magnitude of $g_{AB} \sim 25.5$ mag in a $2''$ aperture, equiva-

TABLE 1
PG1630+377 ABSORBER PROPERTIES

Species	$\log N$ [cm^{-2}] ^a	
	Strong ^b	Weak ^c
H I	16.98 ± 0.06	16.30 ± 0.02
C II	< 13.71	< 13.50
C III	> 13.87	> 13.91
Si II	< 12.42	< 12.38
Si III	> 13.07	> 13.11
Si IV	< 12.93	< 12.89
Mg II	12.19 ± 0.02	< 11.50
O VI	...	14.48 ± 0.03^d

NOTE. — We adopt oscillator strengths from Morton (2003).

^a Strong and weak H I components are integrated over $\Delta v = [-105, +25]$ km s⁻¹ and $\Delta v = [+25, +135]$ km s⁻¹ with respect to $z=0.27395$.

^b Centered at $z=0.27395$.

^c Centered at $z=0.27416$.

^d This is all the detected O VI, integrated over $\Delta v = [-35, +135]$ km s⁻¹. O VI in the strong component velocity range is $\log N(\text{OVI}) = 13.91 \pm 0.04$.

lent to $L \sim 0.005 L_*$ at $z \sim 0.274$. A full description of the LBT imaging will be presented in a future paper.

We selected targets for a preliminary redshift survey based on photometric redshifts of bright galaxies from the Sloan Digital Sky Survey (SDSS). For the three galaxies marked in Figure 1, we obtained longslit spectra with the Keck/LRIS through a $1''$ slit using the

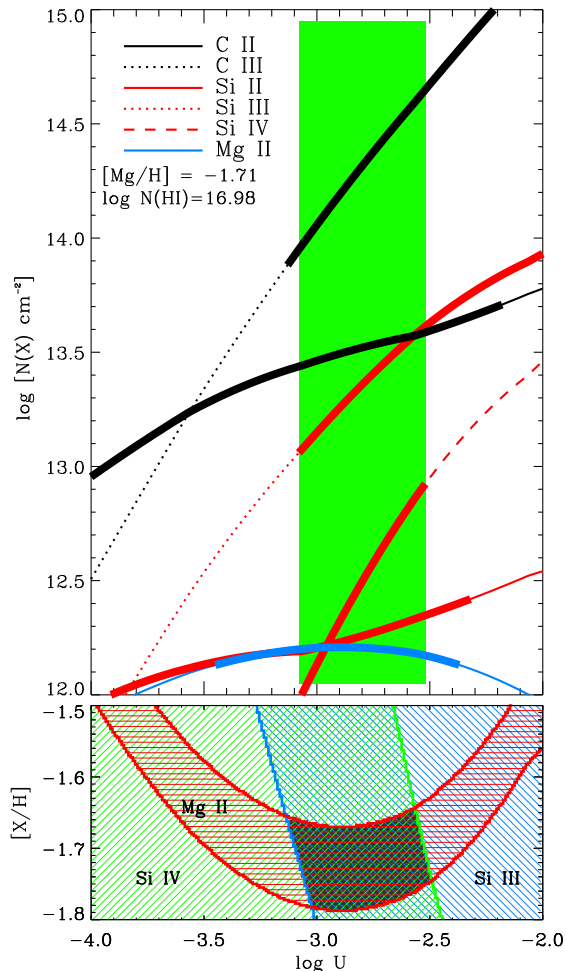


FIG. 4.— The top panel shows the Cloudy-predicted column densities as a function of ionization parameter for the strong component with the metallicity of the gas set to $[\text{Mg}/\text{H}] = -1.71$. The bold portions of the curves show where the model column densities are consistent with the observations. The green band shows the range of ionization parameter for which the models are consistent with our observations. The lower panel shows the metallicities and ionization parameters consistent with the observed columns of the Si and Mg ions. The overlap of these near $[\text{X}/\text{H}] = -1.7$ and $\log U = -3$ to -2.5 is the region allowed by these constraints. The Mg II region includes the uncertainties in H I since these directly affect the $[\text{X}/\text{H}]$ measurements. The detection of Mg II absorption is crucial for determining the metallicity to better than a factor of ~ 3 .

D560 dichroic with the 600/4000 grism (blue side) and 600/7500 grating (red side). This gave spectral coverage between 3000 to 5500 Å (blue side) and 5600 to 8200 Å (red side). On the blue side, binning the data 2×2 resulted in a dispersion of 1.2 Å per pixel and a resolution of $R \sim 1070$ ($\text{FWHM} \sim 280 \text{ km s}^{-1}$). On the red side, the data were binned 2×1 , resulting in a dispersion of 2.3 Å per pixel and a resolution of $\sim 200 \text{ km s}^{-1}$. For strong nebular emission lines from the galaxies we achieved $\text{S/N} \geq 10 \text{ pixel}^{-1}$ with exposure times of $1 \times 900 \text{ s}$ in the blue and $2 \times 410 \text{ s}$ in the red.

The data reduction and calibration (see Werk et al. 2011) were carried out using the LowRedux¹⁰ IDL software package, which includes flat fielding to correct for pixel-to-pixel response variations and larger scale illumi-

nation variations, wavelength calibration, sky subtraction, and flux calibration using the spectrophotometric standard star G191-B2B. We also applied a flux correction to the spectra using SDSS photometry to ensure the flux calibrations of the red and blue side spectra were consistent and to correct for light losses in the 1" slit. To do this we convolved the LRIS spectra with SDSS *ugriz* filter response curves using the IDL code “spec2mag” (see da Silva et al. 2011). We then compared the spectrally-determined apparent magnitudes with the SDSS catalog apparent magnitudes (see Werk et al. 2011) to derive the correction. We corrected the spectra for foreground Galactic reddening using the maps of Schlegel et al. (1998) and assume an intrinsic ratio of $\text{H}\alpha$ to $\text{H}\beta$ of 2.86 to correct for internal reddening, which corresponds to case B recombination at an effective temperature of 10,000 K and electron density of 100 cm^{-3} (Hummer & Storey 1987).

We determined the galaxy redshifts by fitting template spectra to the LRIS spectra using a modified version of the SDSS *zfind* code. Systematic effects (e.g., wavelength calibration) dominate the errors, limiting the accuracy of our measurements to $\sim 25 \text{ km s}^{-1}$. We eliminate one of the candidate hosts (83_19)¹¹ due to its low redshift ($z \sim 0.174$). The other two galaxies have redshifts similar to that of the LLS (see Figure 1) at impact parameters¹² of 37 kpc (296_9) and 140 kpc (75_36). However, the velocity of 75_36 relative to the absorber is likely too high for it to be the associated galaxy: $\Delta v_{75_36} \equiv v_{\text{abs}} - v_{\text{gal}} = -925 \text{ km s}^{-1}$. The velocity separation between 296_9 and the LLS is $\Delta v_{296_9} = -26 \text{ km s}^{-1}$. We identify this galaxy as associated with the LLS. There are a number of other galaxies in the field without spectroscopic redshifts. However, the identification of the LLS with 296_9 is secure for the following reasons. Most importantly, the velocity separation between the absorber and this galaxy is extremely small. It is very unlikely for such a small velocity offset to occur randomly. At the very least, the absorber is associated with the environment with which 296_9 is associated. In addition, all of the galaxies nearer to the QSO sight line than the candidate host are extremely faint with very small angular diameters, consistent with their being high redshift background systems.

We use the observed $\text{H}\alpha$ luminosity of 296_9 with the Calzetti et al. (2010) relationship to estimate a star formation rate of this galaxy, deriving $\text{SFR}_{296_9} = 1.5 M_{\odot} \text{ yr}^{-1}$. The stellar mass of 296_9 is $M_{\star} \sim 2 \times 10^9 M_{\odot}$, derived from SDSS photometry. We determined the oxygen abundance using the R23 metallicity indicator (Pagel et al. 1979) as calibrated by McGaugh (1991). We derive an abundance for 296_9 of $[\text{O}/\text{H}] = -0.20 \pm 0.15$. This estimate places the object near the convergence of the two branches of the R23 diagnostic, thus the systematic errors due to the degeneracy in metallicities associated with the strong line method are small compared to the factor of 30 difference in metallicities seen between

¹¹ The first number in this notation gives the direction in degrees of the galaxy north of east from this QSO line of sight. The second number is the angular distance in arcseconds to the galaxy from the line of sight.

¹² In this paper we assume $H_0 = 72 \text{ km s}^{-1} \text{ Mpc}^{-1}$, $\Omega_m = 0.27$, and $\Omega_{\Lambda} = 0.73$.

¹⁰ <http://www.ucolick.org/~xavier/LowRedux/index.html>

the LLS gas and the galaxy. We used the $[\text{N II}]/[\text{O II}]$ ratio, following Kewley & Ellison (2008), to confirm the derived abundance. The general systematic errors associated with age effects and stellar distributions can be as large as 0.25 dex (Ercolano et al. 2007), but such large effects are still not enough to modify our conclusions. The metallicity, stellar mass, and star formation rate derived for 296_9 place this system on the mean mass-metallicity relationship of Mannucci et al. (2010).

4. THE ORIGIN OF PRIMITIVE GAS IN LYMAN LIMIT SYSTEMS

We have identified a low-redshift, $z_{\text{abs}} \sim 0.274$, LLS with a very low metallicity, $[\text{Mg}/\text{H}] = -1.71 \pm 0.06$, associated with a near-solar metallicity galaxy. The metallicity of the LLS is much lower than the metallicity distribution of damped Lyman- α systems (DLAs) at $z \lesssim 1$ (Kulkarni & Fall 2002; Rao et al. 2005; Wolfe et al. 2005). From a sample of 11 DLAs at $z \lesssim 1$ (see Table 5, Rao et al. 2005), the mean metallicity of these systems is around -0.7 dex; these systems have a large spread in metallicity, but the two lowest values are -1.2 and -1.3 dex. In contrast, such low metallicities do not appear to be the exception for LLSs at $z \lesssim 1$. A perusal of the literature finds 4 out of 8 well-studied LLS at $z \lesssim 1$ have metallicities $[\text{M}/\text{H}] < -1.8$ to ≈ -1.4 (this work, Zonak et al. 2004; Tripp et al. 2005; Cooksey et al. 2008). Recently, Thom et al. (2011) found another strong H I absorber with $\log N(\text{H I}) \sim 16$ having $[\text{M}/\text{H}] < -1.5$. Preliminary results of our ongoing study to expand the number of LLS metallicity measurements at $z \lesssim 1$ appear to confirm that the metallicity distribution of LLSs is different from that of DLAs at similar redshifts, with a high fraction of LLSs having $[\text{M}/\text{H}] \lesssim -1.5$ (N. Lehner et al. 2011, in prep.).

Zonak et al. (2004) and Tripp et al. (2005) argued that a possible origin for these low metallicity LLSs was low metallicity dwarf galaxies. However, the (tentative) high frequency of these primitive LLSs could favor another origin that was not really considered previously. Indeed, since only the tail of the dwarf galaxy metallicity distribution shows such very low abundances, they are unlikely to show up in significant numbers in absorption line studies. That is, the probability a line of sight passing through gas from galaxies like the very low metallicity dwarf galaxy I Zw 18 (Kunth & Sargent 1986) is very small. Furthermore, the relatively low H I column density of the system demonstrates the sight line does not pass through a galaxy. Except for the highest-redshift LLSs in this sample (Zonak et al. 2004), all of these LLSs show at least a sub- L^* galaxy within 100 kpc consistent with being a “host” galaxy. For the present sight line, our deep LBC/LBT images of the field do not show other strong candidates for a galaxy associated with the LLS at $\rho \lesssim 37$ kpc, though our spectroscopic galaxy information is limited.

For the present LLS, we have demonstrated that the likely host galaxy has a metallicity much higher than the LLS, ruling out altogether that the gas in the LLS could originate from this galaxy. We therefore propose instead that this and the low-metallicity LLSs from the literature trace matter infalling onto galaxies, perhaps related to the CMA streams predicted by galaxy formation simulations. The physical properties of the low-metallicity

LLSs are similar to those predicted by CMA models, including the temperature, metallicity, and H I column as well as host galaxy properties such as velocity offset and mass. For the present LLS, the temperature of this LLS is constrained to be $T \leq 3.8 \times 10^4$ K from the b -value derived from our component fit to the H I profiles, consistent with the temperatures predicted by all CMA models. More generally, these LLSs are well modeled by photoionization models that predict temperatures to be about a few times 10^4 K.

The low metallicity of the present and literature systems are consistent with the predictions of Fumagalli et al. (2011), who find cold streams in their simulations have a broad distribution of abundances centered on $\sim 1\%$ solar. These LLSs are likely to have been enriched above primordial levels by previous star formation episodes before streaming into a galaxy. Fumagalli et al. predict the majority of cold streams should be predominantly ionized at $\log N(\text{H I}) \lesssim 19.0$, consistent with the properties of the current sample of LLSs. For our study, we estimate that the stellar mass of the host galaxy is $M_* = 2 \times 10^9 M_\odot$, well below the predicted stellar mass cutoff for CMA host galaxies. While there could always be galaxies hidden underneath the glare of the background QSO that could have contributed the gas making up this LLS, we note that this is also consistent with the CMA simulations. The infalling streams in such models are enriched by small galaxies that will themselves merge with the dominant host galaxy.

Our work highlights the potential importance of H I-selected LLSs as probes of infalling, metal-poor gas. While observations of some LLSs clearly indicate they are related to galactic outflows/winds or galaxy mergers (Jenkins et al. 2005; Lehner et al. 2009; Tumlinson et al. 2011), it is also apparent that the population of LLSs includes very low-metallicity gas with properties very similar to those predicted by CMA models. While the sample of LLSs is still currently small, we will expand it at $z \lesssim 1$ in the near future with the aim to better constrain the metallicity distribution of these systems. Our analysis suggests the best metal species for tracing CMA may be intermediate ions such as C III and Si III (and other ions like O II or O III), as the low ions (C II, Si II, and Mg II) and high ions (Si IV) are suppressed in such low density, low metallicity gas. Kacprzak et al. (2010) have also argued, on the basis of numerical simulations, that the majority of weak Mg II systems ($20 \text{ m}\text{\AA} < W_r(2796) < 300 \text{ m}\text{\AA}$) trace material infalling onto a galaxy. The present LLS has $W_r(2796) = 59 \pm 4 \text{ m}\text{\AA}$, while the metal-poor system studied by Zonak et al. (2004) has $W_r(2796) = 97 \pm 8 \text{ m}\text{\AA}$ – both consistent with this suggestion.

5. SUMMARY

We have presented high-quality UV and optical spectroscopic and imaging observations from COS/*HST*, HIRES/Keck, LRIS/Keck, and LBC/LBT of a LLS with $\log N(\text{H I}) = 17.06 \pm 0.05$ at $z_{\text{abs}} = 0.27395$ along the QSO PG1630+377 and the galaxies in its field of view in order to explore the origin(s) of the LLS at low redshift. The main results of our analysis are as follows:

1. The LLS shows metal line absorption from Mg II, C III, Si III, and O VI. The high S/N of the COS

spectrum allowed us to derive stringent upper limits for several other ions (in particular C II, Si II, and Si IV). These allow a secure metallicity measurement of $[\text{Mg}/\text{H}] = -1.71 \pm 0.06$ for the stronger of the two components in this system due to the tight constraints on the ionization state of the gas. The O VI absorption is mostly associated with the weaker component (at $+50 \text{ km s}^{-1}$ from the stronger absorber) and is likely a result of its interaction with a galaxy halo.

2. Our limited redshift survey of galaxies close on the sky to PG1630+377 shows that there is a $0.3 L_*$ star-forming galaxy projected 37 kpc from the QSO at nearly identical redshift to the LLS ($z = 0.27406$, $\Delta v = -26 \text{ km s}^{-1}$) with near solar metallicity ($[\text{O}/\text{H}] = -0.20 \pm 0.15$). While our spectroscopic survey is extremely limited, the deep LBT images do not suggest another plausible host galaxy at $\rho < 37 \text{ kpc}$.
3. The literature contains several other very low metallicity LLSs at $z \lesssim 1$. While the sample is still small, we find a high frequency ($\sim 50\%$) of $z \lesssim 1$ LLSs have $[\text{M}/\text{H}] \lesssim -1.5$, which appears to differ from the metallicity distribution of DLAs at similar redshifts and from a similar sample size. We propose these very low metallicity LLSs are signa-

tures of infall onto galaxies, perhaps similar to the cold mode accretion predicted by cosmological simulations. The ionization, metallicity, temperature, and host galaxy properties in these simulations are in good agreement with the properties derived from observations of the H I-selected LLSs.

Support for Program number HST-GO-11741 was provided by NASA through a grant from the Space Telescope Science Institute, which is operated by the Association of Universities for Research in Astronomy, Incorporated, under NASA contract NAS5-26555. JCH and JR acknowledge support from NASA grant NNX08AJ31G. TMT and JDM also appreciate support from NASA grant NNX08AJ44G. This work made use of data from the Large Binocular Telescope. The LBT is an international collaboration among institutions in the United States, Italy and Germany. The LBT Corporation partners are: The University of Arizona on behalf of the Arizona university system; Istituto Nazionale di Astrofisica, Italy; LBT Beteiligungsgesellschaft, Germany, representing the Max Planck Society, the Astrophysical Institute Potsdam, and Heidelberg University; The Ohio State University; The Research Corporation, on behalf of The University of Notre Dame, University of Minnesota and University of Virginia.

REFERENCES

- Asplund, M., Grevesse, N., Sauval, A. J., & Scott, P. 2009, *ARA&A*, 47, 481
- Bauermeister, A., Blitz, L., & Ma, C.-P. 2010, *ApJ*, 717, 323
- Birnbom, Y., & Dekel, A. 2003, *MNRAS*, 345, 349
- Bouché, N., et al. 2007, *ApJ*, 671, 303
- Bowen, D. V., & Chelouche, D. 2011, *ApJ*, 727, 47
- Calzetti, D., et al. 2010, *ApJ*, 714, 1256
- Chen, H.-W., & Prochaska, J. X. 2000, *ApJ*, 543, L9
- Chen, H.-W., Wild, V., Tinker, J. L., Gauthier, J.-R., Helsby, J. E., Shectman, S. A., & Thompson, I. B. 2010, *ApJ*, 724, L176
- Cooksey, K. L., Prochaska, J. X., Chen, H.-W., Mulchaey, J. S., & Weiner, B. J. 2008, *ApJ*, 676, 262
- da Silva, R. L., Prochaska, J. X., Rosario, D., Tumlinson, J., & Tripp, T. M. 2011, *ApJ*, 735, 54
- Ercolano, B., Bastian, N., & Stasińska, G. 2007, *MNRAS*, 379, 945
- Faucher-Giguère, C.-A., & Kereš, D. 2011, *MNRAS*, L208
- Ferland, G. J., Korista, K. T., Verner, D. A., Ferguson, J. W., Kingdon, J. B., & Verner, E. M. 1998, *PASP*, 110, 761
- Fumagalli, M., Prochaska, J. X., Kasen, D., Dekel, A., Ceverino, D., & Primack, J. R. 2011, *arXiv:1103.2130*
- Gnat, O., & Sternberg, A. 2007, *ApJS*, 168, 213
- Haardt, F., & Madau, P. 2011, *arXiv:1105.2039*
- Howk, J. C., Ribaldo, J. S., Lehner, N., Prochaska, J. X., & Chen, H.-W. 2009, *MNRAS*, 396, 1875
- Hummer, D. G., & Storey, P. J. 1987, *MNRAS*, 224, 801
- Jenkins, E. B., Bowen, D. V., Tripp, T. M., & Sembach, K. R. 2005, *ApJ*, 623, 767
- Kacprzak, G. G., Churchill, C. W., Ceverino, D., Steidel, C. C., Klypin, A., & Murphy, M. T. 2010, *ApJ*, 711, 533
- Kacprzak, G. G., Churchill, C. W., Barton, E. J., & Cooke, J. 2011, *ApJ*, 733, 105
- Kereš, D., Katz, N., Weinberg, D. H., & Davé, R. 2005, *MNRAS*, 363, 2
- Kewley, L. J., & Ellison, S. L. 2008, *ApJ*, 681, 1183
- Kulkarni, V. P., & Fall, S. M. 2002, *ApJ*, 580, 732
- Kunth, D., & Sargent, W. L. W. 1986, *ApJ*, 300, 496
- Lehner, N., Howk, J. C., Keenan, F. P., & Smoker, J. V. 2008, *ApJ*, 678, 219
- Lehner, N., Prochaska, J. X., Kobulnicky, H. A., Cooksey, K. L., Howk, J. C., Williger, G. M., & Cales, S. L. 2009, *ApJ*, 694, 734
- Mannucci, F., Cresci, G., Maiolino, R., Marconi, A., & Gnerucci, A. 2010, *MNRAS*, 408, 2115
- McGaugh, S. S. 1991, *ApJ*, 380, 140
- Meiring, J. D., et al. 2011, *ApJ*, 732, 35
- Ménard, B., & Chelouche, D. 2009, *MNRAS*, 393, 808
- Morton, D. C. 2003, *ApJS*, 149, 205
- Pagel, B. E. J., Edmunds, M. G., Blackwell, D. E., Chun, M. S., & Smith, G. 1979, *MNRAS*, 189, 95
- Prochaska, J. X., Weiner, B. J., Chen, H.-W., & Mulchaey, J. S. 2006, *ApJ*, 643, 680
- Prochaska, J. X., O'Meara, J. M., & Worseck, G. 2010, *ApJ*, 718, 392
- Rao, S. M., Prochaska, J. X., Howk, J. C., & Wolfe, A. M. 2005, *AJ*, 129, 9
- Ribaldo, J., Lehner, N., & Howk, J. C. 2011, *ApJ*, 736, 42
- Savage, B. D., & Sembach, K. R. 1991, *ApJ*, 379, 245
- Schlegel, D. J., Finkbeiner, D. P., & Davis, M. 1998, *ApJ*, 500, 525
- Sembach, K. R., et al. 2003, *ApJS*, 146, 165
- Songaila, A., & Cowie, L. L. 2010, *ApJ*, 721, 1448
- Spitzer, L. 1978, *New York Wiley-Interscience, Physical Processes in the Interstellar Medium*, 1978. 333 p.
- Stewart, K. R., Kaufmann, T., Bullock, J. S., Barton, E. J., Maller, A. H., Diemand, J., & Wadsley, J. 2010, *arXiv:1012.2128*
- Thom, C., Werk, J. K., Tumlinson, J., Prochaska, J. X., Meiring, J. D., Tripp, T. M., & Sembach, K. R. 2011, *arXiv:1105.4601*
- Tripp, T. M., Jenkins, E. B., Bowen, D. V., Prochaska, J. X., Aracil, B., & Ganguly, R. 2005, *ApJ*, 619, 714
- Tripp, T. M., Sembach, K. R., Bowen, D. V., Savage, B. D., Jenkins, E. B., Lehner, N., & Richter, P. 2008, *ApJS*, 177, 39
- Tumlinson, J., et al. 2011, *ApJ*, 733, 111
- Werk, J. K., Prochaska, J. X., Thom, C., et al. 2011, *arXiv:1108.3852*
- Wolfe, A.M., Gawiser, E., Prochaska, J.X. 2005, *ARA&A*, 43, 861
- Zonak, S. G., Charlton, J. C., Ding, J., & Churchill, C. W. 2004, *ApJ*, 606, 196